CALIPSO observations of near-cloud aerosol properties as a function of cloud fraction

Weidong Yang[1,2], Alexander Marshak[2], Tamás Várnai[2,3], Robert Wood[4]

[1]{Goddard Earth Sciences Technology and Research, Universities Space Research Association, Columbia, MD 21044 USA}

[2]{NASA Goddard Space Flight Center, Greenbelt, MD 20771 USA}

[3]{Joint Center for Earth System Technology, University of Maryland at Baltimore County, Baltimore, MD 21228 USA}

[4]{Department of Atmospheric Sciences, University of Washington, Seattle, WA 98195 USA}

Abstract:

This paper uses spaceborne lidar data to study how near-cloud aerosol statistics of attenuated backscatter depend on cloud fraction. The results for a large region around the Azores show that: (1) far-from-cloud aerosol statistics are dominated by samples from scenes with lower cloud fractions, while near-cloud aerosol statistics are dominated by samples from scenes with higher cloud fractions; (2) near-cloud enhancements of attenuated backscatter occur for any cloud fraction but are most pronounced for higher

cloud fractions; (3) the difference in the enhancements for different cloud fractions is most significant within 5 km from clouds; (4) near-cloud enhancements can be well approximated by logarithmic functions of cloud fraction and distance to clouds.

These findings demonstrate that if variability in cloud fraction across the scenes used to composite aerosol statistics are not considered, a sampling artifact will affect these statistics calculated as a function of distance to clouds. For the Azores-region dataset examined here, this artifact occurs mostly within 5 km from clouds, and exaggerates the near-cloud enhancements of lidar backscatter and color ratio by about 30%. This shows that for accurate characterization of the changes in aerosol properties with distance to clouds, it is important to account for the impact of changes in cloud fraction.

1. Introduction

Aerosol-cloud interactions can induce significant changes in the optical and microphysical properties of clouds and aerosols, and are therefore highly important for understanding solar radiative forcing and climate change. In examining aerosol-cloud interactions, many observational studies have found positive correlations between cloud fraction and Aerosol Optical Depth (AOD), or solar reflectance, and/or lidar backscatter [e.g., Ignatov et al., 2005; Loeb and Manalo-Smith, 2005; Matheson et al., 2005; Zhang et al., 2005; Kaufman and Koren, 2006; Koren et al., 2007; Loeb and Schuster, 2008; Su et al., 2008; Redemann et al., 2009, Chand et al. 2012]. Other studies found that clear areas near clouds have higher lidar backscatter (or solar reflectance) values than areas far from clouds do, thus forming areas called "twilight zone" or "transition zone" [e.g., Platt et al 1971; Lu et al., 2003; Charlson et al., 2007; Koren et al., 2007]. Such zones are characterized by a gradual increase in the reflected signal as the measurements approach a cloud [Tackett and Di Girolamo, 2009; Várnai and Marshak, 2011 and 2012; Yang et al., 2012; Várnai et al., 2013]. Physically, such zones are thought to contain aerosols swollen in the humid air that surrounds clouds, aerosols generated or processed in the clouds, and undetected small and/or thin cloud pieces [e.g., Hoppel et al., 1986; Clarke et al., 2002; Su et al., 2008; Koren et al., 2008, 2009; Bar-Or et al., 2010, 2011 and 2012].

In addition, it was found that instrumental limitations [Qiu et al., 2000], cloud contamination [e.g., Zhang et al., 2005] and three-dimensional (3D) solar radiative processes [e.g., Wen et al., 2007; Marshak et al., 2008; Kassianov and Ovchinnikov, 2008] in cloudy environments can also contribute significantly to the apparent

70 enhancements observed near clouds. Analysis of the contributing factors in the near-
71 cloud enhancements is needed to help better understand both cloud-aerosol interactions
72 and the direct radiative effect of aerosols [e.g. Várnai et al., 2013].
73
74 Studies of aerosol near-cloud behavior often involve statistics taken from large datasets
75 that cover large areas and a long time span. For example, in a global yearlong dataset,
76 Várnai and Marshak (2012) found an anti-correlation between median distance to cloud
77 and cloud fraction, though they also noted that cloud structure also influences the
78 distribution of distance to cloud. One may argue that far-from-clouds clear-sky regions
79 can occur only in areas with low cloud fractions while the statistics of close-to-clouds
80 regions are likely to be strongly influenced by areas with higher cloud fractions.
81 Therefore, AOD (as well as reflectance or lidar backscatter) may be higher close to
82 clouds than far from clouds simply because of the well-documented positive correlations
83 between AOD and cloud fraction [e.g., Loeb and Manalo-Smith, 2005; Chand et al.,
84 2012]. As a result, the statistically increasing scattering enhancement as clouds are
85 approached could potentially merely be a consequence of these correlations, rather than
86 reflecting any physical changes near clouds.
87
88 The above argument can be illustrated through a simple example. We consider a dataset
89 in which aerosol samples are obtained in three regions with different cloud fractions A_1,
90 A_2, and A_3, and we assume that $A_3 > A_2 > A_1$ (Fig. 1a). Let us further assume that clear
91 sky AODs in each region remain constant with respect to distance to clouds, and have
92 values of τ_1, τ_2 and τ_3 for each of the regions with A_1, A_2, *and* A_3, respectively (Fig. 1b).

93 The assumption that $\tau_3 > \tau_2 > \tau_1$ while $A_3 > A_2 > A_1$ is well consistent with the observed
94 correlation between AOD and cloud coverage.
95
96 Combining data from all regions together, the average AOD (symbol $\bar{\tau}$) at distance x
97 from clouds is the weighted sum of $\tau(x, A)$ over all cloud fraction (A) values, i.e.

98 $$\bar{\tau}(x) = \int_0^1 \tau(x, A) n(x, A) dA \ . \quad (1)$$

99 Here the weight $n(x, A)$ is the ratio of the number of samples with A at x to the total
100 number of all samples with all A's at x, and so $\int_0^1 n(x, A) dA = 1$. As Várnai and Marshak
101 [2012] found some anti-correlation between distance to cloud and cloud fraction, we can
102 expect to find progressively more samples with high cloud fraction as we approach
103 clouds. Therefore in this simple example, it is plausible to assume that weights of given
104 cloud fractions vary as shown schematically in Fig. 1a. In Fig. 1a $n(x, A_1)$ is an increasing
105 function of x while $n(x, A_3)$ is a decreasing one. Because low cloud fraction is associated
106 with low AOD, the changes in the sample weights lead to an apparent enhancement of $\bar{\tau}$
107 closer to clouds (black curve in Fig. 1b). This reveals that statistical results may behave
108 differently from our initial assumption of distance-independent, constant AOD for
109 individual scenes. In the following, we call the apparent enhancement described above as
110 *sampling effect*/*sampling artifact* for the reason that it is induced by variation of sampling
111 weights of cloud fractions, instead of the variation of near-cloud aerosol properties.
112
113

114 This raises the questions: *What is the true statistical near-cloud behavior? Do the*
115 *enhancements observed in earlier studies come entirely from this effect?* To address
116 these questions, we first analyze the samples' cloud fraction dependent features as a
117 function of distance to cloud using a CALIPSO data over the Atlantic Ocean. Next, we
118 examine the near-cloud behaviors of aerosols for various cloud fractions. Finally, we
119 introduce a method for studying near-cloud aerosol properties using satellite
120 observations, and estimate the fraction of enhancements due to the statistical cloud
121 fraction-sampling effect.
122
123 **2. Data and methodology**
124 In this study we analyze data from a large region over the Atlantic Ocean near the Azores
125 (25°-45°N, 20°-37°W). This region is well suited for this study because it is rich in low-
126 level marine boundary layer clouds types and cloud fractions and is ideal site for studying
127 interactions between cloud, aerosol and precipitation [e.g. Wood, 2009; Rémillard et al.
128 2012, Dong et al., 2014, Wood et al. 2014].
129
130 We examine this region using data from the CALIOP (Cloud-Aerosol Lidar with
131 Orthogonal Polarization) lidar on board the CALIPSO (Cloud Aerosol-Lidar and Infrared
132 Path finder Satellite Observations) satellite, which was launched in 2006 [e.g., Winker et
133 al., 2007]. CALIOP provides range-resolved cloud and aerosol data along its track,
134 including attenuated total lidar backscatter at 532 nm and 1064 nm, and perpendicularly
135 polarized lidar backscatter at 532 nm. CALIOP operational algorithms (currently in

136 Version 3) use this data along with altitude and latitude information for feature
137 identification and classification [Liu et al., 2009; Omar et al., 2009].
138
139 Similarly to earlier studies [e.g. Várnai and Marshak, 2011 and 2012; Yang et al., 2012;],
140 we reduce the noise due to background illumination and sampling by using only
141 nighttime data and by combining observations from a three-year period (2006.6.21-
142 2009.6.21) over the entire study region.
143
144 In this study, we examine the 532 nm attenuated total lidar backscatter coefficient β (the
145 ratio of vertically integrated backscatter within an aerosol layer over layer thickness) and
146 the attenuated total color ratio χ (ratio of total backscatter at 1064 nm over that at 532
147 nm) at a horizontal resolution of 333 m. The backscatter coefficient is used for
148 examining variations in the optical density of aerosol layers, while the color ratio is
149 related to changes in the size of spherical particles [Liu et al., 2000, Liu et al., 2004,
150 Cattrall et al., 2005 and Omar et al., 2005]. To be consistent with earlier studies [Várnai
151 and Marshak, 2011 and 2012; Yang et al., 2012], we examine aerosol properties in cloud-
152 free columns as a function of distance to the nearest cloud edge—the closest point where
153 a cloud is detected in the 0.333 km or 1 km cloud mask. While the 5-km resolution cloud
154 mask is not used for defining the nearest cloud edge, aerosol data is used only when the
155 5 km cloud mask (most sensitive to thin clouds) also indicates a fully cloud-free column
156 at all altitudes. Also, we use aerosol data only if the nearest cloud is of liquid water
157 phase with a cloud top below 3 km, and if the top of the aerosol layer is below 5 km.
158 Moreover, we exclude data from clear-sky segments shorter than 3 km in order to reduce

159 the amount of data possibly contaminated by undetected clouds. To further reduce the
160 influence from undetected clouds, aerosol data are used only if a particle layer is
161 identified as an aerosol layer with high confidence [Liu et al., 2009], with CAD (cloud-
162 aerosol discrimination) values larger than 70. (Additional tests showed that using higher
163 CAD thresholds does not change the basic observed behaviors and our conclusions).
164
165 In this paper, we define cloud fraction as the ratio of the number of 0.333 km cloudy
166 profiles (with clouds in either the 0.333 km or 1 km resolution cloud mask) to the total
167 number of 0.333 km profiles within 15 km from it. Since CALIOP can only detect
168 clouds and aerosols along the 1D track, clouds off the track are unknown and can cause
169 uncertainties in estimating the true distance to clouds and cloud fraction [e.g., Astin et al.
170 2001]. However, the cloud fractions estimated based on 1D tracks and 2D images should
171 be statistically similar; as a result, the cloud fraction dependent features found in 1D can
172 be a good approximation of the features in 2D. Finally, Várnai and Marshak (2012) found
173 that near-cloud behaviors are highly correlated when considering 1D or 2D distances to
174 clouds.
175
176
177 **3. Results**
178 The distribution of the total number of aerosol samples $N(x, A)$ as a function of distance
179 to clouds x and cloud fraction A is shown in Fig. 2. Figure 2a indicates that the sample
180 number distributions vary with cloud fraction in a way that depends on how close the
181 samples are to clouds: At farther distances, samples are distributed over a narrow range

182 of small cloud fractions (see the purple curve); while at closer distances, samples are
183 from a much wider cloud fraction range and mostly from higher cloud fractions of 0.3-0.5
184 (e.g., the red curve). This behavior is consistent with the assumptions used in the
185 introduction (Fig. 1a). Figure 2b shows the way the sample fraction ($n(x, A)$ in Eq. (1))
186 changes with distance to cloud for various ranges of cloud fraction. The plot shows that
187 for low cloud fractions (red curve) sample fractions increase dramatically with distance,
188 while for high cloud fractions (e.g., black curve) sample fractions decrease with distance.
189 We note that this behavior is qualitatively similar to the one assumed in Fig. 1a. These
190 features arise from the fact that far-from-cloud samples are more easily found in areas of
191 smaller cloud fractions than larger ones.
192
193 The near-cloud properties observed at specific cloud fractions are shown in Fig. 3. The
194 most important findings are as follows. (1) The enhancements of near-cloud backscatter
195 and color ratio occur for *all* cloud fractions and are most pronounced for higher cloud
196 fraction values, as shown in Figs. 3a and 3b. This feature indicates that the mechanisms
197 causing the near-cloud enhancements (such as aerosol humidification and cloud
198 contamination) are present in all clear sky conditions but are most prominent in high
199 cloud fraction cases. (2) At a given distance away from cloud, both the attenuated total
200 backscatter coefficient β and color ratio χ are increasing functions of cloud fraction and
201 are more sensitive to cloud fraction at closer distances (Figs. 3c and 3d). In contrast, the
202 positive correlations of backscatter coefficient and color ratio with cloud fraction are not
203 significant at larger distances to clouds ($> \sim 5$ km). This indicates that clouds have a
204 strong influence on their surroundings, but the range of influence may be limited to about

5 km, at least for this dataset. (3) As indicated by the high regression coefficients R, the enhancements in near-cloud aerosol properties can be well approximated by the logarithmic functions, i.e.:

$$\beta(x, A) \approx a_1(A)\text{-}b_1(A)*\log(x) \quad (2)$$

and

$$\chi(x, A) \approx a_2(A)\text{-}b_2(A)*\log(x) \quad (3)$$

where, in this study, A ranges from 0.1 to 1 and x is the dimensionless distance to clouds normalized by the resolution of 1 km, with $x \geq 1$. Let us analyze the trend in coefficients a and b in the logarithmic approximation of the attenuated total backscatter coefficient $\beta(x, A)$ (see Eq. (2) and Figs. 3a and 3c). (The coefficients for the attenuated total color ratio $\chi(x, A)$ behave similarly (Figs. 3b and 3d).) First, $a_1(A)=\beta(x=1,A)$ describes the near-cloud behavior while $b_1(A)$ is the degree of dependence on the distance to clouds; both are functions of cloud fraction A (Fig. 3a). As expected, both a_1 and b_1 are increasing functions of A, i.e., the larger A the bigger β near clouds and the stronger changes in β with the distance from cloud. Note that for the smallest cloud fraction (red curve), a_1 and b_1 are both the smallest and show the weakest dependence on distance from cloud.

Figure 3c shows that the attenuated backscatter $\beta(x, A)$ as a function of A can be also well approximated by a logarithmic function,

$$\beta(x, A) \approx a_3(x)\text{-}b_3(x)*|\log(A)| \quad (4)$$

for $x \geq 1$ and $A \geq 0.1$. Here coefficient $a_3(x)$, as a function of x, is equal to the asymptotic value of β if A=1 and $b_3(x)$ describes the degree of cloud fraction dependence for each distance from cloud. We can see that both functions a_3 and b_3 are decreasing; in other

words, the bigger the distance from cloud the weaker dependence of aerosol properties on cloud fraction (compare red and magenta curves in Fig. 3c or 3d). An approximation similar to Eq. (4) is also valid for the attenuated total color ratio χ (see Fig. 3d).

The presence of near-cloud enhancements for all cloud fractions in Fig. 3 confirm that the enhancement in composite statistics comes, at least in part, from physical changes near clouds. Meanwhile, the dependence of $n(x, A)$ on x in Fig. 2 indicates that a sampling artifact is also likely to affect the composite statistics (see Fig. 1).

In order to estimate the impact of sampling effect on the composite statistics, we resample our data to make the distribution of cloud fraction ($n(x,A)$) used in Eq. (1) the same for any distance to clouds. We specify this distribution to be the one observed at distance x_0, a large distance beyond which aerosol properties vary little with cloud fraction. In this study we use x_0=10 km (Figure 3). This resampling will make the distribution of cloud fraction to be $n(x,A) = n(x_0,A)$ for any $x \geq 1$, thus removing the impacts on composite statistics combining data for all cloud fractions.

Figure 4 compares the β and χ values *with* and *without* applying the proposed resampling method. It shows that near-cloud enhancements become significantly smaller with the resampling (black curves) than they were without the resampling (red curves), and that the differences are mostly within 5 km from clouds. Here the near-cloud enhancement of β and χ is defined as the relative increase over the value at 20 km beyond which aerosols are less affected by clouds (e.g. Twohy, et al., 2009). The inserts show that the fraction of

enhancement by the sampling effect also vary with distance to clouds; for this dataset it can reach 30% at the distance of 1 km.

It should be noted that the sampling effect depends on location and season. The example technique of using a pre-selected cloud fraction distribution at a certain far-from-cloud distance (x_0) is not the only method for removing the artifacts caused by near-cloud variations in cloud fraction distributions. The key here is to use identical cloud fraction distributions at all distances, so that the sampling artifact caused by variations in cloud fraction distributions in Eq. (1) can be removed.

4. Concluding remarks

Several studies [e.g., Tackett and Di Girolamo, 2009; Várnai and Marshak, 2011; Yang et al., 2012; Várnai et al., 2013] have found that aerosol properties vary systematically with distance to the nearest cloud, pointing to the presence of a wide transition zone around clouds. In this paper we examine whether the apparent enhancement of aerosol backscatter and color ratio observed near clouds is indeed a sign of a such transition zone, or it is just a manifestation of the well-documented correlation between aerosol properties and cloud fraction [e.g., Loeb and Manalo-Smith, 2005; Chand et al., 2012]. This question arises because clear-sky sample populations used in the statistical analysis can be different near clouds and far from clouds: Near-cloud samples are more likely to come from areas/times with higher cloud fractions, while far-from-cloud samples are more likely to come from areas/times of lower cloud fractions.

To answer this question, we analyzed the cloud fraction-dependence of near-cloud sample numbers and aerosol optical properties using CALIOP nighttime data from a wide region around the Azores. The results indicate that as expected, near-cloud aerosol statistics are dominated by data for higher cloud fractions, while far-from-cloud statistics are dominated by data for lower cloud fractions. At the same time, however, near-cloud enhancements remain large even if we use samples only from a narrow cloud fraction interval, especially if this cloud fraction is high. In addition, it is found that the cloud fraction-dependence of near-cloud behaviors can be well approximated by logarithmic functions (Eqs. (2)-(4)).

These findings indicate that near-cloud aerosol statistics are affected by cloud fraction distributions changing with distance to cloud. The effects can be removed if, for all distances to cloud, we resample the data to the same cloud fraction distribution. When resampling our entire dataset to the cloud fraction distribution observed at 10 km away from clouds, the near-cloud enhancement of our original dataset was reduced by up to 30%, with most reduction occurring within 5 km from clouds.

This result suggests that systematic changes in the near-cloud transition zone are real but somewhat weaker than previously reported, and that understanding the statistics of near-cloud aerosol properties requires a consideration of changes in cloud fraction.

Acknowledgements:

We gratefully acknowledge support for this research by the NASA CALIPSO project supervised by Charles Trepte and by the NASA award NNX13AQ35G, as well as the support from the US Department of Energy (DOE) Office of Science (BER) under grants DE-SC0005457 and DE-SC0006865MOD0002. We also thank Alex Kostinski, Alexei Lyapustin, and Larry Di Girolamo for helpful discussions and suggestions. The CALIPSO data were obtained from the NASA Langley Research Center Atmospheric Sciences Data Center.

References:

Astin, I., L. Di Girolamo, and H. M. van dePoll (2001), Bayesian confidence intervals for true fractional coverage from finite transect measurements: Implications for cloud studies from space, *J. Geophys. Res.*, 106(D15), 17303–17310, doi:10.1029/2001JD900168.

Bar-Or, R.Z., I. Koren, and O. Altaratz (2010), Estimating cloud field coverage using morphological analysis, *Environ. Res. Lett.*, 5, doi: 10.1088/1748-

9326/5/1/014022.

Bar-Or, R. Z., O. Altaratz, and I. Koren (2011), Global analysis of cloud field coverage and radiative properties, using morphological methods and MODIS observations, *Atmos. Chem. Phys.*, 11, 191-200.

Bar-Or, R. Z., I. Koren, O. Altaratz, and E. Fredj (2012), Radiative properties of humidified aerosols in cloudy environment, Atmos. Res., 118, 280-294

Cattrall, C., J. Reagan, K. Thome, and O. Dubovik (2005), Variability of aerosol and spectral lidar and backscatter and extinction ratios of key aerosol types derived from selected Aerosol Robotic Network locations, *J. Geophys. Res.*, 110, p. D10S11, http://dx.doi.org/10.1029/2004JD005124

Chand, D., R. Wood, S. Ghan, M. Wang, M. Ovchinnikov, P. J. Rasch, S. Miller, B. Schichtel, and T. Moore (2012), Aerosol optical depth enhancement in partly cloudy conditions. *J. Geophys. Res.*, 117, D17207, doi:10.1029/2012JD017894

Charlson, R. J., A.S. Ackerman, F. A.-M. Bender, T.L. Anderson, and Z. Liu (2007), On the climate forcing consequences of the albedo continuum between cloudy and clear air, *Tellus*, 59B, pp. 715–727 http://dx.doi.org/10.1111/j.1600-0889.2007.00297.x

Clarke, A. D., S. Howell, S., P. K. Quinn, T. S. Bates, J. A. Ogren, E. Andrews, A. Jefferson, and A. Massling (2002), INDOEX aerosol: A comparison and summary of chemical, microphysical, and optical properties observed from land, ship, and aircraft, *J. Geophys. Res*. 107(D19), 8033.

Dong, X., B. Xi, A. Kennedy, P. Minnis, and R. Wood (2014), A 19-Month Record of Marine Aerosol–Cloud–Radiation Properties Derived from DOE ARM Mobile

343 Facility Deployment at the Azores. Part I: Cloud Fraction and Single-Layered
344 MBL Cloud Properties, *J. Climate*, **27**, 3665–3682. doi:
345 http://dx.doi.org/10.1175/JCLI-D-13-00553.1
346 Hoppel, W. A., G. M. Frick, and R. E. Larson (1986), Effect of nonprecipitating clouds
347 on the aerosol size distribution in the marine boundary layer, *Geophys. Res. Lett.*
348 13, 125–128.
349 Ignatov, A., P. Minnis, N. Loeb, B. Wielicki, W. Miller, S. Sun-Mack, D. Tanre, L.
350 Remer, I. Laslo, and E. Geier (2005), Two MODIS aerosol products over ocean
351 on the Terra and Aqua CERES SSF, *J. Atmos. Sci.* 62, 1008–1031.
352 Kassianov, E.I., and M. Ovtchinnikov (2008), On reflectance ratios and aerosol optical
353 depth retrieval in the presence of cumulus clouds, *Geophy. Res. Lett.* 35, L06311.
354 Kaufman, Y.J., and I. Koren (2006), Smoke and pollution aerosol effect on cloud cover,
355 Science 313: 655–658
356 Koren, I., L. A. Remer, Y. J. Kaufman, Y. Rudich, and J. V. Martins (2007), On the
357 twilight zone between clouds and aerosols, *Geophys. Res. Lett*. 34, L08805.
358 Koren, I., J. V. Martins, L. A. Remer, and H. Afargan (2008), Smoke invigoration versus
359 inhibition of clouds over the Amazon, *Science* 321, 946–949.
360 Koren, I., G. Feingold, H. Jiang, and O. Altaratz (2009), Aerosol effects on the inter-
361 cloud region of a small cumulus cloud field, *Geophys. Res. Lett.*, 36, L14805,
362 doi:10.1029/2009GL037424.
363 Liu, Z., P. Voelger, and N. Sugimoto (2000), Simulations of the observation of clouds
364 and aerosols with the Experimental Lidar in Space Equipment system, *Appl. Opt.*,
365 39, pp. 3120–3137.

366 Liu, Z., M.A. Vaughan, D.M. Winker, C.A. Hostetler, L.R. Poole, D. Hlavka, W. Hart,
367 and M. McGill (2004), Use of probability distribution functions for discriminating
368 between cloud and aerosol in lidar backscatter data, *J. Geophys. Res.*, 109, p.
369 D15202 http://dx.doi.org/10.1029/2004JD004732
370 Liu, Z., M. Vaughan, D. Winker, C. Kittaka, B. Getzweich, R. Kuehn, A. Omar, K.
371 Powell, C. Trepte, C. Hostetler (2009), The CALIPSO lidar cloud and aerosol
372 discrimination: Version 2 algorithm and initial assessment of performance, *J.*
373 *Atmos. Oceanic Technol.* 26, 1198–1213.
374 Loeb, N. G., and N. Manalo-Smith (2005), Top-of-atmosphere direct radiative effect of
375 aerosols over global oceans from merged CERES and MODIS observations, *J.*
376 *Climate* 18, 3506–3526.
377 Loeb, N. G., and G. L. Schuster (2008), An observational study of the relationship
378 between cloud, aerosol and meteorology in broken low-level cloud conditions, *J.*
379 *Geophys. Res.* 113, D14214.
380 Lu, M. L., J. Wang, A. Freedman, H. H. Jonsson, R. C. Flagan, R. A. McClatchey, and J.
381 H. Seinfeld (2003), Analysis of humidity halos around trade wind cumulus
382 clouds, *J. Atmos. Sci.* 60, 1041–1059.
383 Marshak, A., G. Wen, J. A. Coakley Jr., L. A. Remer, N. G. Loeb, and R. F. Cahalan
384 (2008), A simple model for the cloud adjacency effect and the apparent bluing of
385 aerosols near clouds, *J. Geophys. Res*. 113, D14S17.
386 Matheson, M. A., J. A. Coakley Jr., and W. R. Tahnk (2005), Aerosol and cloud property
387 relationships for summertime stratiform clouds in the northeastern Atlantic from
388 AVHRR observations, *J. Geophys. Res.* 110, D24204.

389 Omar,A.H., J.-G. Won, D.M. Winker, S.-C. Yoon, O. Dubovik, and M.P. McCormick
390 (2005), Development of global aerosol models using cluster analysis of Aerosol
391 Robotic Network (AERONET) measurements. *J. Geophys. Res.*, p. D10S14
392 http://dx.doi.org/10.1029/2004JD004874
393 Omar, A.H., D.M. Winker, M.A. Vaughan, Y. Hu, C.R. Trepte, R.A. Ferrare, K.-P. Lee,
394 C.A. Hostetler, C. Kittaka, R.R. Rogers, R.E. Kuehn, and Z. Liu (2009), The
395 CALIPSO automated aerosol classification and lidar ratio selection algorithm. *J.*
396 *Atmos. Oceanic Technol.*, 26, pp. 1994–2014.
397 http://dx.doi.org/10.1175/2009JTECHA1231.1
398 Platt, C. M. R. and D. J. Gambling (1971), Laser radar reflexions and downward infrared
399 flux enhancement near small cumulus clouds, *Nature*, 232, 182–185
400 Perry, K. D., and P. V. Hobbs (1996), Influences of isolated cumulus clouds on the
401 humidity of their surroundings, *J. Atmos. Sci.* 53, 159–174.
402 Qiu, S., G. Godden, X. Wang, and B. Guenther (2000), Satellite-Earth remote sensor
403 scatter effects on Earth scene radiometric accuracy, *Metrologia* 37, 411-414.
404 Redemann, J., Q. Zhang, P. B. Russell, J. M. Livingston, and L. A. Remer (2009), Case
405 Studies of Aerosol Remote Sensing in the Vicinity of Clouds, *J. Geophys. Res.*
406 114, D6.
407 Rémillard, J., P. Kollias, E. Luke, and R. Wood (2012), Marine boundary layer cloud
408 observations at the Azores, *J. Clim.*, **25**, 7381–7398
409 Su, W., G. L. Schuster, N. G. Loeb, R. R. Rogers, R. A. Ferrare, C. A. Hostetler, J. W.
410 Hair, and M. D. Obland (2008), Aerosol and cloud interaction observed from high
411 spectral resolution lidar data, *J. Geophys. Res.* 113, D24202.

412 Tackett, J. L., and L. D. Girolamo (2009), Enhanced aerosol backscatter adjacent to
413 tropical trade wind clouds revealed by satellite-based lidar, *Geophys. Res. Lett.*
414 36, L14804.
415 Twohy, C. H., Coakley Jr., J. A., Tahnk, W. R., 2009. Effect of changes in relative
416 humidity on aerosol scattering near clouds. J. Geophys. Res. 114, D05205.
417 Várnai, T., and A. Marshak (2011), Global CALIPSO observations of aerosol changes
418 near clouds, *IEEE Rem. Sens. Lett.* 8, 19-23.
419 Várnai, T., and A. Marshak (2012), Analysis of co-located MODIS and CALIPSO
420 observations near clouds, *Atmos. Meas. Tech.,* 5, 389-396, 2012
421 doi:10.5194/amt-5-389-2012
422 Várnai, T., A. Marshak, and W. Yang (2013), Multi-satellite aerosol observations in the
423 vicinity of clouds, *Atmos. Chem. Phys*, *13*, 3899-3908 doi:10.5194/acp-13-3899-
424 2013
425 Wen, G., A. Marshak, R. F. Cahalan, L. A. Remer, and R. G. Kleidman,, (2007), 3-D
426 aerosol-cloud radiative interaction observed in collocated MODIS and ASTER
427 images of cumulus cloud fields, *J. Geophys. Res.* 112, D13204.
428 Winker, D. M., W. Hunt, and M. McGill (2007), Initial performance assessment of
429 CALIOP, *Geophys. Res. Lett.* 34, L19803.
430 Wood, R. (2009), Clouds, Aerosol, and Precipitation in the Marine Boundary Layer
431 (CAP-MBL), DOE/SC-ARM-0902, 23 pp. [Available online at
432 http://www.arm.gov/publications/programdocs/doe-sc-arm-0902.pdf?id**5**94.]
433 Wood, R., M. Wyant, C. S. Bretherton, J. Rémillard, P. Kollias, J. Fletcher, J. Stemmler,
434 S. deSzoeke, S. E. Yuter, M. Miller, D. Mechem, G. Tselioudis, C. Chiu, J. Mann,

435 E. O'Connor, R. Hogan, X. Dong, M. Miller, V. Ghate, A. Jefferson, Q. Min, P.
436 Minnis, R. Palinkonda, B. Albrecht, E. Luke, C. Hannay and Y. Lin (2014),
437 Clouds, Aerosol, and Precipitation in the Marine Boundary Layer: An ARM
438 Mobile Facility Deployment, *Bull. Amer. Meteorol. Soc.*, doi:
439 http://dx.doi.org/10.1175/BAMS-D-13-00180.1.
440 Yang, W., A. Marshak, T. Várnai, and Z. Liu (2012), Effect of CALIPSO cloud aerosol
441 discrimination (CAD) confidence levels on observations of aerosol properties
442 near clouds, *Atmos. Res.,* Vol. 116, 15, pp. 134–141. DOI:
443 10.1016/j.atmosres.2012.03.013
444 Zhang, J., J. S. Reid, and B. N. Holben (2005), An analysis of potential cloud artifacts in
445 MODIS over ocean aerosol optical thickness product, *Geophys. Res. Lett.* 32,
446 L15803.
447

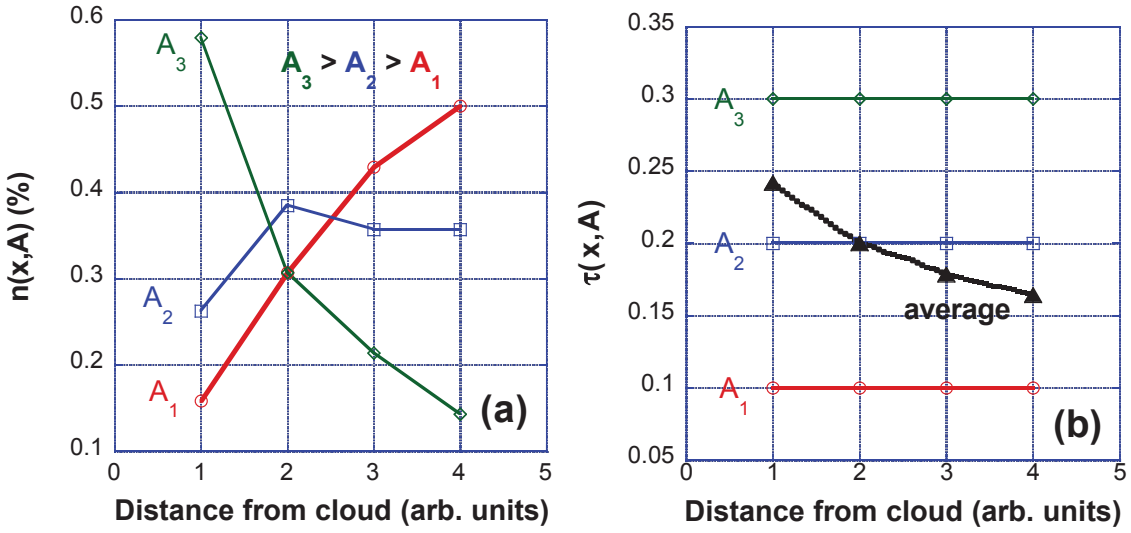

Fig. 1. Schematic illustration of the potential effect of sampling on the averaged AOT as a function of distance to cloud, x. (**a**) probability density function $n(x,A)$ [$\int n(x,A)dA = 1$] for three cloud fractions $A_1 < A_2 < A_3$. (**b**) average AOT, [$\bar{\tau}(x) = \int \tau(x,A)n(x,A)dA$] assuming AOT for each cloud fraction is constant: $\tau(x,A_1)=0.1$, $\tau(x,A_2)=0.2$, $\tau(x,A_3)=0.3$.

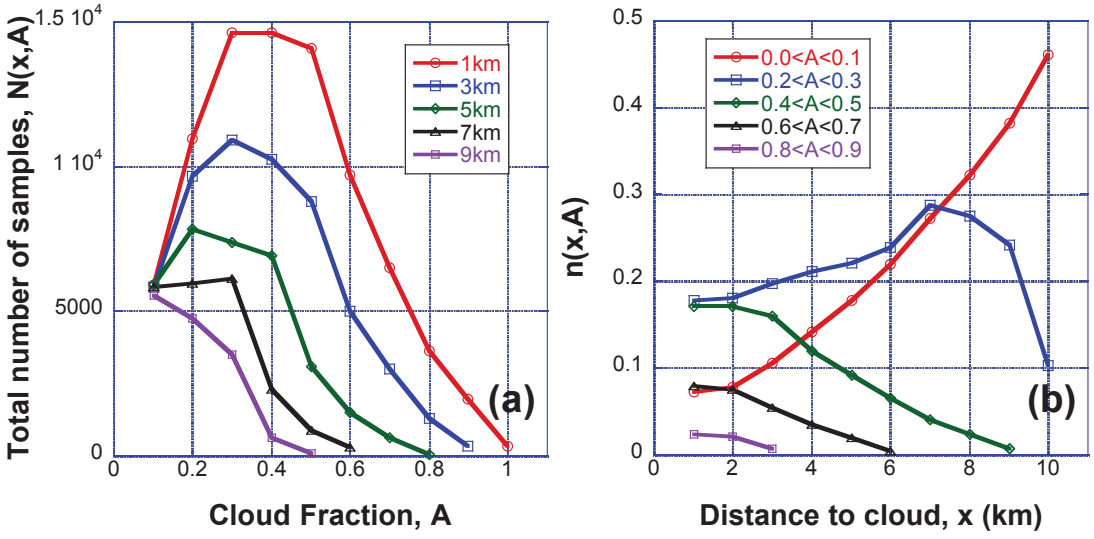

Fig. 2. Sample numbers used in the analysis. (**a**) Total number of samples, $N(x,A)$, for each distance to cloud x, as a function of cloud fraction A. (**b**) Probability density function $n(x,A) = N(x,A) / \int N(x,A)dA$ as a function of distance to cloud.

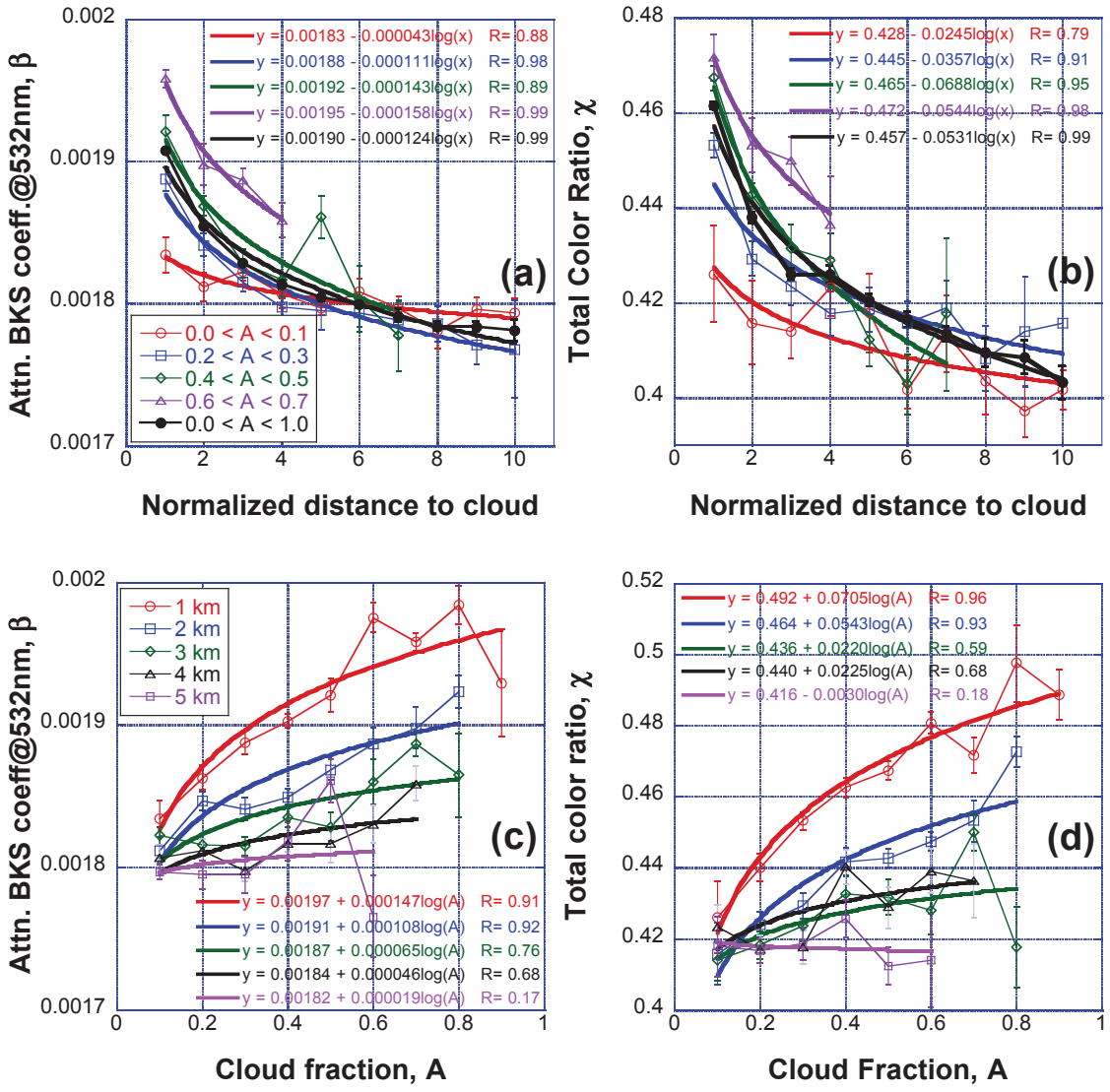

Fig. 3. Medians of attenuated total backscatter coefficient β and total color ratio χ as a function of normalized distance to cloud x and cloud fraction A. (**a**) Median attenuated total backscatter coefficient vs. normalized distance to cloud and a log fit: $\beta(x,A) \approx a_1(A) - b_1(A)*\log(x)$ with $x \geq 1$, for four intervals of cloud fraction (0.0-0.1, 0.2-0.3, 0.4-0.5, and 0.6-0.7) and the average one (0.0-1.0). Note that the distance to cloud is normalized by resolution of 1 km and both $a_1(A)=\beta(x=1,A)$ and $b_1(A)$ are increasing functions of A. (**b**) The same as in panel (a) but for attenuated total color ratio. Log fits are $\chi(x,A) \approx a_2(A) - b_2(A)*\log(x)$ with $x \geq 1$; $a_2(A)= \chi(x=1,A)$. (**c**) Median attenuated total backscatter

coefficient vs. cloud fraction and a log fit: $\beta(x,A) \approx a_3(x)-b_3(x)*|\log(A)|$ with $1 \geq A \geq 0.1$ for five distances to cloud ranging from 1 km to 5 km. Note that both $a_3(x)=\beta(x,A=1)$ and $b_3(A)$ are decreasing functions of x. (**d**) The same as in panel (c) but for total color ratio. Log fits are $\chi(x, A) \approx a_4(x)-b_4(x)*|\log(A)|$ with $1 \geq A \geq 0.1$; $a_4(x)=\chi(x,A=1)$. The curves in panels (a)-(d) have been truncated for large distances to clouds and/or large cloud fractions because the sample numbers after the truncated point are either zero or extremely low leading to large uncertainties.

485

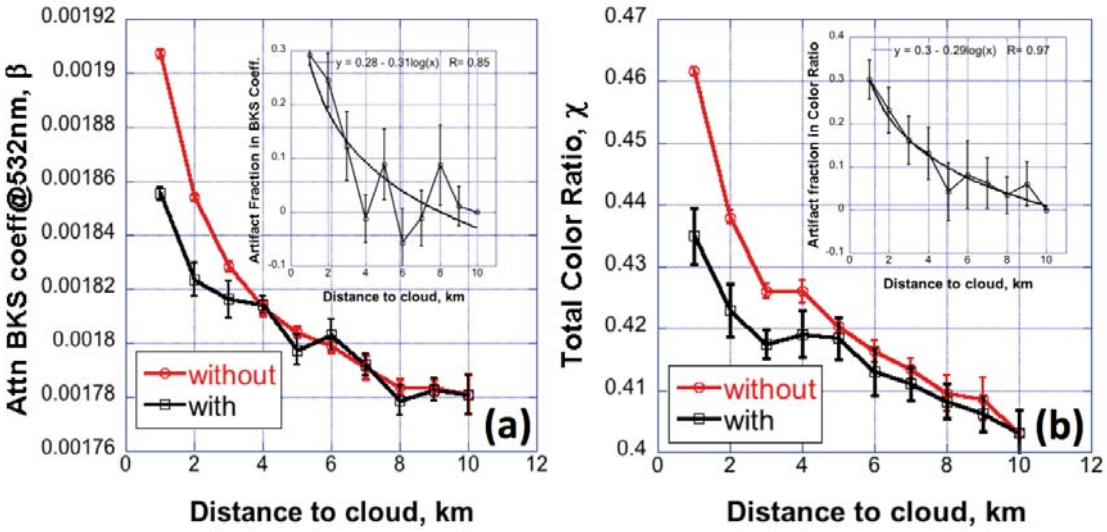

486

487 **Fig. 4**. Medians of attenuated total backscatter coefficient and color ratio as a function of

488 distance to cloud without and with removing the sampling effect. Inserts show sampling

489 effect fraction (1-'*with*'/'*without*'). (**a**) Median attenuated total backscatter coefficient.

490 (**b**) Median attenuated total color ratio.

491

492

493